RSC Advances

ROYAL SOCIETY OF CHEMISTRY

www.rsc.org/advances

RSC Advances

PAPER

Synthesis of Surfactant-Free SnS Nanoplates in an Aqueous Solution

Received 00th January 20xx,
Accepted 00th January 20xx

DOI: 10.1039/x0xx00000x

www.rsc.org/

Heeseung Yang,[a] Chang-Eun Kim,[a] Anupam Giri,[b] Aloysius Soon,[a]* Unyong Jeong,[b]*

We report a synthetic route to produce surfactant-free SnS nanoplates with the *Pbnm* crystal structure. The process is quick and environment-friendly, accomplished in a mild aqueous condition. The synthesis involves two steps, formation of an intermediate tin oxide hydroxide ($Sn_6O4(OH)_4$) gel and its chemical transformation into SnS nanoplates in the presence of sulfide precursor (Na_2S). we found that addition of small amount of PVP during the chemical transformation results in the formation of cubic SnS with the *Cmcm* crystal structure. We discuss about the development of the crystal structures on the basis of density functional theory (DFT) calculations on the structure-energy relationship of SnS nanostructures. The optical properties of the SnS nanoplates and nanocubes are compared.

Introduction

Two-dimensional (2D) layered materials have drawn widespread interest because of their unique electronic, chemical, physical properties, and their potential applications associated with lateral anisotropy.[1-3] Among various 2D layered materials, narrow band gap IV–VI series of semiconducting materials have attracted great attention owing to their wide range of optoelectronic applications such as for photovoltaics and near-infrared detectors etc.[4,5]

Among the variety of IV–VI 2D materials, SnS has been of intensive interest for its unique semiconducting and optical properties in addition to high natural abundance and low toxicity.[6] Bulk SnS has both an indirect and direct band gaps of approximately 1.1 eV and 1.3 eV, respectively. It has been widely used for photodetectors,[7,8] photocatalysts,[9] and lithium ion batteries.[10] Although there have been many literatures reporting successful control of the shape and stability of SnS nanostructured materials,[8,11-14] most of the synthetic procedure involves the use of polymeric surfactants or capping agents.[15-17] Hydrocarbon molecules containing amine functional groups such as oleylamine have been commonly used as surfactants for the synthesis of SnS nanostructures.[18, 19] Those surfactant-assisted approaches often suffer the cumbersome removal of the surfactants, which is required for their optoelectronic applications. Even a small amount of surfactant at the surfaces of nanomaterials changes their electronic characteristics and causes contact resistance.[20,21] Therefore, achieving a surfactant-free synthesis can potentially circumvent those issues and provide a significant advancement in the applications involving 2D nanostructured materials.

This study suggests a robust synthesis to produce surfactant-free SnS nanoplates. The synthesis is based on a simple concept of using a surfactant-free intermediate, tin oxide hydroxide ($Sn_6O_4(OH)_4$), which can be easily transformed into SnS nanoplates in the presence of S source. More interestingly, upon addition of a small amount of polyvinylpyrrolidone (PVP) as a surfactant together with S source, SnS nanocubes were produced instead of nanoplates. In order to understand the energetic origin of crystal formation, we have performed density-functional theory (DFT) calculations.[22] This study also compares the optical properties of the SnS nanoplates and nanocubes.paragraph text follows directly on here.

Experimental

Materials. Tin(II) chloride ($SnCl_2$, 98%), ammonium hydroxide solution (28%), sodium sulfide nonahydrate (98%), and polyvinylpyrrolidone (PVP, Mw = 55000) were purchased from Sigma-Aldrich. All chemical reagents were used as received without further purification.

Preparation of tin oxide hydroxide ($Sn_6O_4(OH)_4$) intermediate. $SnCl_2$ (2.26 g) was dissolved in 10 mL DI-water. 100 mL ammonium hydroxide solution was added into the $SnCl_2$ solution, and the mixture was vigorously stirred for 1 h at 60 ^oC. After 1 h, the resulting milky white precipitate in the solution was centrifuged and washed with ethanol and water three times. The precipitate was dried in a vacuum desiccator for 12 h before its further use.

[a] *Department of Materials Science and Engineering, Yonsei University, 50 Yonsei-Ro, Seodaemun-Gu, Seoul 120-749, Korea*
[b] *Department of Materials Science and Engineering, POSTECH, 77 Cheongam-Ro, Nam-Gu, Pohang, Gyeongbuk 790-784, Korea.*
* Corresponding Authors: ujeong@postech.ac.kr, aloysius.soon@yonsei.ac.kr.

Electronic Supplementary Information (ESI) available: [Digital images of the reaction mixture according to time, TEM images of PVP effect and UV-vis-NIR absorption spectra of the nanocubes and nanoplates of SnS are included.]. See DOI: 10.1039/x0xx00000x

Synthesis of surfactant-free SnS nanoplates. The dried $Sn_6O_4(OH)_4$ powder (0.1g) was dispersed in 40 mL of DI-water (in a round bottom flask) under ultrasonication. Then the solution was heated up to 100 ^oC under nitrogen atmosphere. In a separate vial, sodium sulfide (0.2g) was dissolved in 10 mL DI-water and the solution was injected into tin oxide hydroxide powder suspension at 100 ^oC. The solution color immediately changed from milky white to dark brown. The reaction was kept for 1 h to complete the reaction. After the reaction, the precipitate was washed with ethanol and water for three times to remove unreacted precursors.

Synthesis of SnS nanocubes. PVP (0.2 g) was dissolved in 10 mL DI-water. This PVP solution was poured into the tin oxide hydroxide suspension at room temperature. The mixture solution was heated up to 100 ^oC under nitrogen atmosphere. Then dissolved sodium sulfide solution (in 10 mL DI-water) was injected into the mixture solution of tin oxide hydroxide and PVP at 100 ^oC. After 1 h, the precipitate was collected by centrifugation and washed three times with ethanol and water before drying it in a vacuum desiccator.

Characterization. Nanostructures of the products were analyzed by scanning electron microscope (SEM, JEOL JSM-7001F) and transmission electron microscope (TEM, JEOL 2100F) at 200 kV acceleration voltage. The crystal structures were characterized by x-ray diffraction (XRD, Rigaku II D/MAX) and selected-area electron diffraction pattern from TEM. The ultraviolet–visible absorption of the SnS nanocrystals was measured with a UV–vis spectrophotometer (JASCO V-500).

DFT calculation. In order to investigate thermodynamically preferred SnS crystal, the DFT calculations were carried out with the Vienna ab initio Simulations Package (VASP 5.3) code.[23,24] We first calculated energies in the vacuum environment. The ion-electron interactions were obtained via the projector augmented wave (PAW) method,[25, 26] and the approximation to the exchange-correlation was made using the Perdew, Burke, and Ernzerhof (PBE) functional.[27] The electronic wave functions were expanded in a plane-wave basis set with a kinetic energy cutoff of 500 eV. The k-space integration was performed using a gamma-centered (8×3×8) grid in the Brillouin zone for both Pbnm and Cmcm phases of bulk SnS, (6×6×1) for the Cmcm SnS(010) surface, (4×2×1) for the Cmcm SnS(101) surface, and (4×2×1) for the Pbnm SnS(111) surface. A Methfessel-Paxton smearing of 0.1 eV was used to improve the convergence of the calculations and the total energy was extrapolated back to zero temperature. We employed the implicit solvation method as implemented in VASP sol code.[28] We used different relative permittivity (εr) values, εr = 80.0 for the water environment, and εr =3.0 for the PVP surfactant environment, respectively.

Results and discussion

Scheme 1 summarizes the synthesis procedure used in this study, via the formation of an intermediate product of Sn(II). Aqueous solution of $SnCl_2$ was mixed with a basic solution of ammonium hydroxide (pH = 9.2), followed by vigorous magnetic stirring for 1 h at 60 ^oC. Under the basic condition, $SnCl_2$ rapidly hydrolyses and forms a white precipitate within 1 h. The precipitate was identified as tin oxide hydroxide ($Sn_6O_4(OH)_4$) sol. All the oxygen atoms are joined by hydrogen bonds in a regular cubic structure and are structurally related to the cyclic $Sn_3(OH)_4^{2+}$ cation.[29,30] The formation of $Sn_6O_4(OH)_4$ intermediate can be explained on the basis of the following two reactions.

$$\mathbf{3\,SnCl_2 + 4\,NH_4OH \rightarrow [Sn_3(OH)_4]^{2+}\cdot 2Cl^- + 4NH_4Cl} \quad (1)$$

$$\mathbf{2[Sn_3(OH)_4]^{2+}\cdot 2Cl^- \rightarrow Sn_6O_4(OH)_4 + 4\,HCl} \quad (2)$$

The $Sn_6O_4(OH)_4$ was centrifuged and washed, then dried in oven. The dry powder was redispersed in DI water and the solution was heated at 100^oC. Upon injecting Na_2S as a sulfide source, the intermediate $Sn_6O_4(OH)_4$ was chemically transformed into SnS nanoplates without any surfactant, while it was transformed into SnS nanocubes in the presence of PVP surfactant.

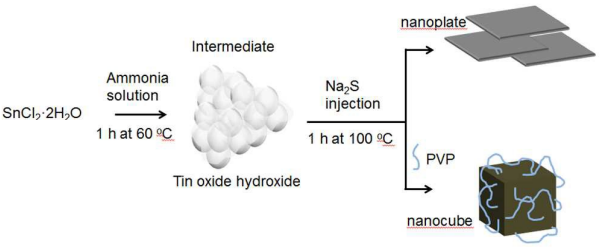

Scheme 1. Schematic illustration of the formation of SnS nanoplates and nanocubes.

Figure 1A shows a TEM image of the as-prepared intermediate, which was irregular nanoparticle aggregate. **Figure 1B** shows the X-ray diffraction (XRD) pattern of the intermediate, where all the diffraction peaks are matched with the crystal structure of tin oxide hydroxide ($Sn_6O_4(OH)_4$) (JCPDS 84-2157).[31] $Sn_6O_4(OH)_4$ crystals were stable in the atmospheric environment. Any by-product such as SnO phase was not detected in the XRD result.

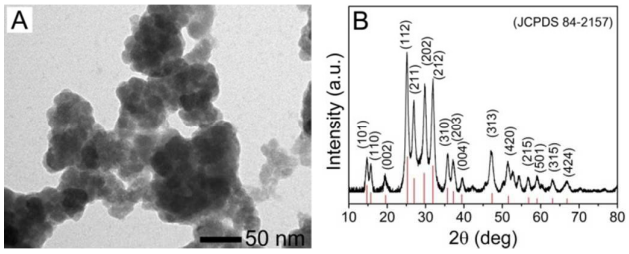

Figure 1. TEM image (A) and powder XRD pattern (B) of $Sn_6O_4(OH)_4$ particles used as intermediate Sn precursors

It has been proven that a salt with a higher solubility product (K_{sp}) is thermodynamically unstable than those with lower K_{sp} values; hence, it can be transformed into other salt having lower K_{sp} values.[32] Since SnS has a lower K_{sp} values (3.2×10^{-28}) than its oxide

(5.7×10^{-27}) or hydroxide (5×10^{-26}) counterpart in neutral water condition,[33,34] Sn compounds in forms of hydroxides or oxides are converted to SnS in the presence of S^{2-} anions. It is notable that the chemical transformation needs excess amount of S^{2-} source because the solubility product differences between SnS and its oxide forms are not large enough to guarantee complete conversion. Upon addition of excess amount of Na_2S salt (0.65 mM, which is about 3 times excess compared to the Sn precursor) in the $Sn_6O_4(OH)_4$ solution, $Sn_6O_4(OH)_4$ was transformed into SnS,

$$\mathbf{Sn_6O_4(OH)_4 + 6Na_2S + 4H_2O \rightarrow 6SnS + 12NaOH} \quad (3)$$

This chemical transformation has been reported recently, although the process used oleic acid and oleylamine as solvent and surfactant.[35] The process in this study is advantageous over the past reports in that the reaction is surfactant free, simple, and productive in massive amount. Furthermore, the process is environmentally friendly as it involves a moderate reaction temperature in an aqueous solution.

The morphologies and crystal structures of the as-synthesized SnS nanomaterials were characterized with SEM, TEM, and XRD**. Figure 2A** represents the SnS orthorhombic crystal structure consisting of distinct layers that are bound through weak van der Waals bonding along the c-axis. Sn and S are bound by partial ionic bonding in the lateral direction within each layer. Because of this anisotropic bonding character, SnS nanocrystals grow preferentially into 2D nanoplates (**Figures 2B and 2C**).[14]

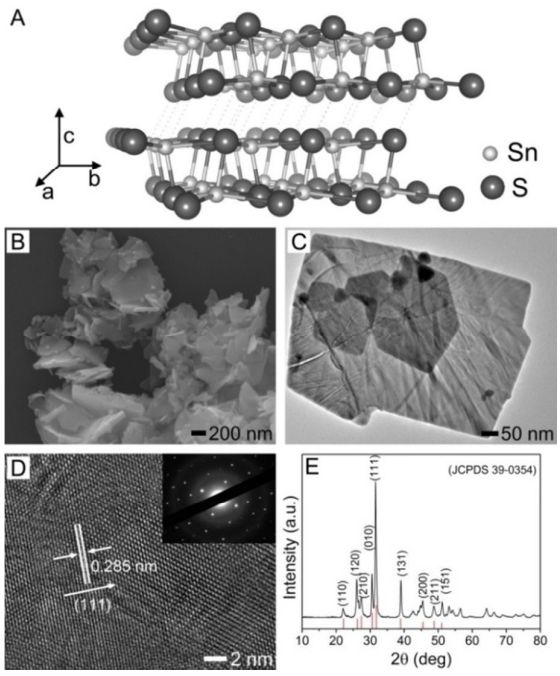

Figure 2. (A) Schematic modeling of layered structure of SnS nanoplates (Pbnm). FE-SEM and TEM images of as-synthesized SnS nanoplates (B and C, respectively). (D) A HR-TEM image of the SnS nanoplates plane and inset image is electron diffraction pattern of SnS nanoplates. (E) Powder XRD patterns of SnS nanoplates.

The average thickness and the lateral dimension of the SnS nanoplates were 20 nm and 380 nm, respectively. The nanoplates were dispersed well in water and ethanol, which is owing to the ionic interaction between surface atoms and polar solvent molecules even in the absence of any surfactant. HR-TEM image of the SnS nanoplate is shown in **Figure 2D**. A lattice spacing of 0.285 nm indicates the directional growth of the nanoplates along [111] direction. The selected area electron diffraction (SAED) pattern of SnS nanoplates (inset in **Figure 2D**) was identical at different spots, which indicates the nanoplates are single crystalline. Figure 2E shows the XRD pattern of the nanoplates where all the diffraction peaks are indexed to the orthorhombic SnS in *Pbnm* space group (JCPDS 39-0354 *Pbnm*).[36-38] The presence of an intense XRD peak corresponding to (111) plane is consistent with HR-TEM result (**Figure 2D**).

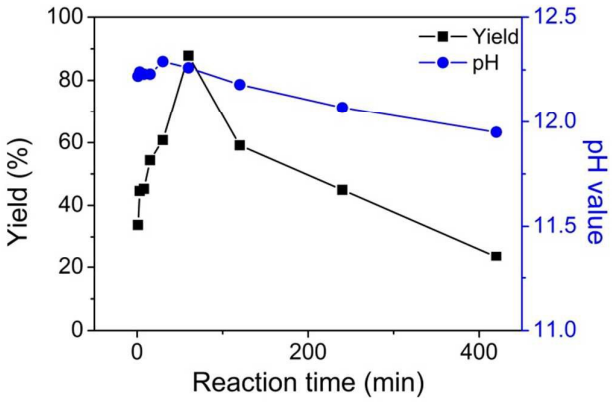

Figure 3. Variation of reaction yield (black square) and pH (blue circle) of the reaction medium as a function of time.

During the synthesis of SnS nanoplates after addition of S^{2-} precursor into the $Sn_6O_4(OH)_4$ suspension, the product yield increased abruptly during the first 10 min (~ 50%) and it slowly increased to reach a maximum (88%) after 1 h (black square symbols in **Figure 3**). The color of the reaction solution turned dark brown immediately within 1 min after injecting Na_2S and the color was maintained during several hours. This fast color change indicates abrupt nucleation and growth of SnS nanocrystals. As the reaction time elapsed further, the product yield continuously decreased. During the reaction, the morphology of the SnS product was the same nanoplates, as shown from TEM images obtained at 20 min and 240 min of reaction times (Figure S1). The color of the reaction mixture became transparent in 24 h (Figure S2). To investigate the mechanistic details of this reaction, we monitored the change in pH of the reaction mixture (blue circle symbols in **Figure 3).** The pH of the reaction mixture decreased with time along with the decrease of product yield. As expressed in Eq.3, the reaction generates NaOH during the formation of SnS nanoplates, which caused increase of pH from 10 to 12.2 until the product yield reached its maximum at 1 h. The simultaneous decrease of reaction

yield and pH after 1 h reaction suggests dissolution of SnS by reaction with OH^-.[39]

$$\mathbf{2SnS + 3OH^- \rightarrow [SnS_2]^{2-} + [Sn(OH)_3]^-} \quad (4)$$

We examined the transparent supernatant solution after collecting the nanoplates by centrifugation (Figure S2). The dissolved $Sn(OH)_3^-$ ion and Na^+ ion formed $NaSn(OH)_3$ salt which made the solution turbid.[40] The supernatant solution became more turbid as the reaction time to form SnS over 1 h was longer, which confirms the etching of SnS nanoplates.

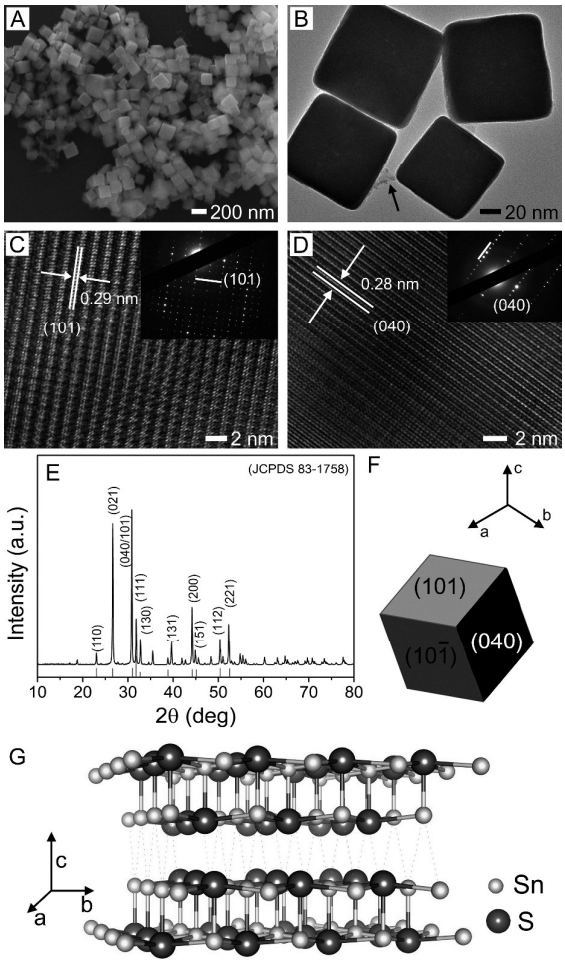

Figure 4. FE-SEM and TEM images of as-synthesized SnS nanocubes (A and B, respectively). The black arrow in (B) indicates tin oxides that were not completely transformed into SnS crystal. (C and D) HR-TEM image of SnS nanocubes and insert shows the corresponding electron diffraction pattern. (E) XRD results of as-synthesized SnS nanocubes. (F) Schematic illustration of each facet of cube structure. (G) Schematic modeling of layered structure of SnS nanocubes (*Cmcm*).

Antonie et al. demonstrated the synthesis and formation mechanism of SnS nanoplates according to various organic surfactants.[41] We investigated the effects of surfactant on the structural development of SnS during the transformation from $Sn_6O_4(OH)_4$ into SnS. We added PVP in the suspension of $Sn_6O_4(OH)_4$ in water and added excess amount of Na_2S. Color of the reaction solution turned dark brown after 5 min, which was longer than the SnS nanoplate synthesis (less than 1 min) without PVP surfactant. This slow color change indicates the crystal nucleation and growth at the initial stage was slower in the presence of PVP surfactant. We have found that the product was well-defined nanocubes instead of nanoplates. **Figures 4A and 4B** exhibit SEM and TEM images of the as-synthesized nanocubes. The edge length of the nanocubes ranged 170 - 200 nm. It is notable that only nanoplates were produced when the concentration of PVP was less than 0.01 wt% (0.5 mg), meanwhile only nanocubes were obtained when the concentration was larger than 0.1 wt% (10 mg). In the concentrations of 0.03 ~ 0.05 wt% PVP solution, we found mixtures of nanoplates and nanocubes, the smaller concentration produced less fraction of nanocubes. The relevant images are shown in the supporting information (Figure S3).

Figure 4C and 4D show the HR-TEM images and electron diffraction patterns from two different cubic faces of the nanocubes. The facets can be identified with the lattice spacing and the corresponding diffraction pattern. The lattice spacings were 0.29 nm and 0.28 nm, which represent the (101) and (040) facets, respectively.[42,43] **Figure 4E** shows the XRD pattern of the nanocubes, where the peaks are mostly matched with the space group of *Cmcm* symmetry, also known as the zinc blende structure. Unidentified small peaks are considered to result from the $Sn_6O_4(OH)_4$ intermediate whose transformation into SnS was not completed, as indicated with an arrow in Figure 4B. Based on the XRD and electron diffraction patterns, Figure 4F shows schematic illustration of nanocube which has different facets along the zone axis. The crystal structure was *Cmcm* (**Figure 4G**) in which the S and Sn elements are positioned in the same plane without any tilted angle. The SnS nanocubes were not etched out even 24 h reaction, which is contrary to the continuous etching in SnS nanoplates after 1 h reaction.

In order to check the thermodynamic preference of the SnS crystals, the DFT calculations were carried out with the Vienna *ab initio* Simulations Package (VASP 5.3) code.[23,24] We first calculated energies in the vacuum environment. To assess the preference of the formation of cubic geometry *Cmcm*, we calculated the energy difference (ΔE) between the nanoplate (*Pbnm*) and the nanocube (*Cmcm*), $\Delta E \equiv \Delta E(Pbnm) - \Delta E(Cmcm)$. ΔE was composed of bulk energy difference (ΔE_{bulk}) and surface energy difference (ΔE_{surf}), $\mathbf{\Delta E = \Delta E_{surf} - \Delta E_{bulk}}$. ΔE_{bulk} and ΔE_{surf} are plotted as a function of nanoparticle size (**Figure 5A**). The aspect ratio (*r*) for the *Pbnm* nanoplate was taken as the average dimension from the experimental result (i.e., a thickness of 20 nm and a width of 500 nm, *r* = 20/500). The geometric dimensions were determined from the volume data, while, in turn, the surface energy contributions were then determined by the geometric dimensions. Thus, all the quantities could be expressed as a function of the volume of the nanocrystals. The DFT results indicate that ΔE_{bulk} destabilizes the cubic *Cmcm* phase, but ΔE_{surf} favors the phase in **Figure 5A**. The

formation of the *Cmcm* cubic nanoparticles is favored over the formation of SnS nanoplates at a small size regime (< ~120 nm), which is because the surface energy contribution is dominant over the bulk energy contribution. To explicitly express the thermodynamic driving force of forming the *Cmcm* cubic phase at very small size regime, we divided the ΔE by the total number of SnS formula units in our model and plotted it as a function of the SnS nanocube size, as seen in **Figure 5B**. Here, it clearly shows there is indeed a strong thermodynamic driving force for this nanocubic preference at very small sizes. However, the *Pbnm* phase is favored as the volume becomes larger than ~120 nm for the same aspect ratio of the nanoplates. The calculation agrees with the experimental results.

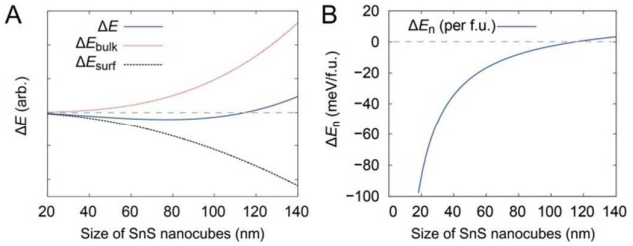

Figure 5. DFT-based phenomenological model: (A) Energy difference between the *Pbnm* nanoplate and the *Cmcm* cubic phases of SnS, $\Delta E \equiv \Delta E(Pbnm) - \Delta E(Cmcm)$, as a function of the size of the cubic particle. ΔE is composed of the bulk contribution (ΔE_{bulk}) and the surface contribution (ΔE_{surf}). The volume of nanoplates were the same with the nanocubes and the aspect ratio was fixed at 20/500. (B) Normalized energy difference, ΔE_n as a function of the size of the cubic particle, showing ΔE divided by the number of the SnS formula unit in the nano particle.

It is worthy to note that this DFT-based phenomenological model does not explicitly include the population statistics of the nanoparticles in a batch. From the experimental results, the morphology during chemical transformation was strongly affected by the presence of the PVP surfactant, as mentioned above in details. We examined the consequences of solvation due to PVP capping agent or pure water with the implicit solvation model.[28] The surface energies were calculated with dielectric constants of PVP and water (ε = 3.0 for PVP and ε = 80.0). With the same aspect ratio (*r* = 20/500), we found that the difference in surface energy due to solvation effect did not drastically modify the trend found from the results obtained in the vacuum environment. As a result, our simple implicit solvation model leads to the same preference of the *Cmcm* phase in both pure water and PVP environment at the regions of small volume. To explain why the *Cmcm* cubic phase is not found in the pure water environment, may require more large-scale simulation e.g. the explicit treatment of the solvent environment and/or molecular dynamics simulation. We tried to investigate whether the *Cmcm* phase transforms into the *Pbnm* phase or not as the volume grows larger than a critical size. Unfortunately, the formation of nanoplates was too fast to track the possible phase transition, which is left as a future work. Relatively, the formation of nanocubes could be tracked microscopically. It followed conventional nucleation and growth mechanism.

The UV-vis absorption behavior of the SnS nanoplates and nanocubes are compared in **Figure 6**. For the SnS nanoplates, the absorption in the UV range decreased and showed a maximum at around 570 nm in the visible region. The nanoplates showed extended absorption in the lower energy near IR region of the spectrum. For the SnS nanocubes, a wide range absorption was observed from UV to 600 nm wavelength, and the absorption dropped abruptly without meaningful absorption in the near IR region (Figure S4). These results suggest that the wide UV-vis-Near IR absorption of the nanoplates can be utilized for the development of near-infrared detectors, photoconductors, and photovoltaic materials.

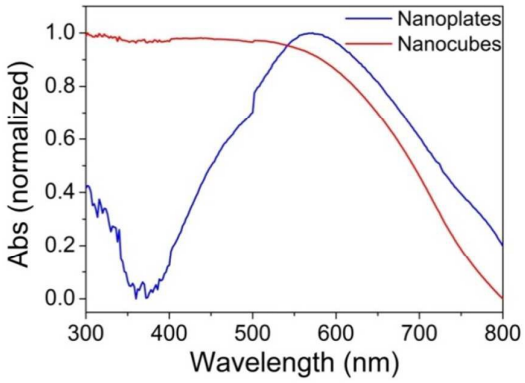

Figure 6. UV-vis-NIR absorption spectrum of SnS nanoplates (black) and SnS nanocubes (red).

Conclusions

A novel synthesis is developed for the preparation of surfactant-free SnS nanoplates in an aqueous solution. It took advantages of the dispersion capability of the SnS nanoplates owing to the their negative charges when dispersed in polar solvents and the easy chemical transformation of $Sn_6O_4(OH)_4$ into SnS crystals. DFT calculation for a vacuum environment indicates that the *Cmcm* cubic phase of SnS is more stable when the volume of nanocrystal is small, but the *Pbnm* nanoplate phase is preferred as the volume of the crystal is larger than a critical size. In synthesis, the SnS nanocubes were obtained in the presence of PVP, however, the SnS nanoplates were produced in pure water without any surfactant. There might be a phase transition from the nanocubes to nanoplates in pure water, but the formation of nanoplates were too fast to track the possible transition. Although the thermodynamic investigation on the nanoplate formation is left as a future study, this simple synthetic procedure to produce surfactant-free SnS nanoplates offers a wide range of possibilities, especially in optical and optoelectronic applications.

Acknowledgements

This research was supported partly by Samsung Research Funding Center of Samsung Electronics under Project Number SRFC-MA1301-07.

Notes and references

1 A. K. Geim and K. S. Novoselov, *Nat. Mater.*, 2007, ***6***, 183.
2 X. Huang, Z. Yin, S. Wu, X. Qi, Q. He, Q. Zhang, Q. Yan, F. Boey and H. Zhang, *Small*, 2011, ***7***, 1876.
3 Y. Min, G. D. Moon, C.-E. Kim, J.-H. Lee, H. Yang, A. Soon, and U. Jeong, *J. Mater. Chem. C*, 2014, ***2***, 6222.
4 A. H. Souici, N. Keghouche, J. A. Delaire, H. Remita, A. Etcheberry and M. Mostafavi, *J. Phys. Chem. C*, 2009, ***113***, 8050.
5 S. G. Hickey, C. Waurisch, B. Rellinghaus and A. Eychmüller, *J. Am. Chem. Soc.*, 2008***, 130***, 14978.
6 P. D. Antunez, J. J. Buckley and R. L. Brutchey, *Nanoscale*, 2011, ***3***, 2399.
7 Z. Deng, D. Cao, J. He, S. Lin, S. M. and Lindsay, Y. Liu, *Acs Nano*, 2012, ***6***, 6197.
8 J.Chao, Z. Wang, X. Xu, Q. Xiang, W. Song, G. Chen, J. Hu and D. Chen, *RSC Advances*, 2013, ***3***, 2746.
9 J. Chao, Z. Xie, X. Duan, Y. Dong, Z. Wang, J. Xu, B. Liang, B. Shan, J. Ye, D. Chen and G. Shen, *Crystengcomm*, 2012, ***14***, 3163.
10 A. M. Tripathi and S. Mitra, *RSC Advances*, 2014, ***4***, 10358.
11 Y. Zhang, J. Lu, S. Shen, H. Xu and Q. Wang, *Chem. Comm.*, 2011, ***47***, 5226.
12 N. Koteeswara Reddy, M. Devika, Q. Ahsanulhaq, and K. R. Gunasekhar, *Cryst. Growth Des.*, 2010, ***10***, 4769.
13 B. K. Patra, S. Sarkar, A. K. Guria and N. Pradhan, *J. Phys. Chem. Lett.*, 2013, ***4***, 3929.
14 A. Walsh and G. W. Watson, *J. Phys. Chem. B*, 2005, ***109***, 18868.
15 X. Liu, Y. Li, B. Zhou, X. Wang, A. N. Cartwright and M. T. Swihart, *Chem. Mater.*, 2014, ***26***, 3515.
16 Z. Liu, D. Xu, J. Liang, J. Shen, S. Zhang and Y. Qian, *J. Phys. Chem. B*, 2005, ***109***, 10699.
17 E. Lifshitz, M. Bashouti, V. Kloper, A. Kigel, M. S. Eisen and S. Berger, *Nano Lett.*, 2003, ***3***, 857.
18 E. C. Greyson, J. E. Barton and T. W. Odom, *Small*, 2006, ***2***, 368.
19 Z. Deng, D. Han and Y. Liu, *Nanoscale*, 2011, ***3***, 4346.
20 D. V. Talapin, J.-S. Lee, M. V. Kovalenko and E. V. Shevchenko, *Chem. Rev.*, 2009, ***110***, 389.
21 V. A. Akhavan, M. G. Panthani, B. W. Goodfellow, D. K. Reid and B. A. Korgel, *Opt. Express*, 2010, ***18***, A411.
22 R. Zhao, S. J. Lee, I. H. Son, H. Lee and A. Soon, *Appl. Surf. Sci.*, 2013, ***265***, 339.
23 G. Kresse and J. Furthmuller, *Comp. Mater. Sci.*, 1996, ***6***, 15.
24 G. Kresse and J. Furthmuller, *Phys. Rev. B*, 1996, ***54***, 11169.
25 G. Kresse and D. Joubert, *Phys. Rev. B*, 1999, ***59***, 1758.
26 P. E. Blochl, *Phys. Rev. B*, 1994, ***50***, 17953.
27 J. P. Perdew, K. Burke and M. Ernzerhof, *Phys. Rev. Lett.*, 1996, ***77***, 3865.
28 K. Mathew, R. Sundararaman, K. Letchworth-Weaver, T. A. Arias and R. G. Hennig, *J. Chem. Phys.*, 2014, ***140***, 084106-1.
29 R. S. Tobias, *Acta Chem. Scand*, 1958, ***12***, 198.
30 W. D. Honnick and J. J. Zuckerman, *Inorg. Chem.*, 1976, ***15***, 3034.
31 H. Uchiyama and H. Imai, *Cryst. Growth Des.*, 2007, ***7***, 841.
32 G. D. Moon, S. Ko, Y. Min, J. Zeng, Y. Xia and U. Jeong, *Nano Today*, 2011, ***6***, 186.
33 J. A. Olmsted and G. M. Williams, *Chemistry 5 ed.*, Wiley, 2006.
34 A. B. Garrett and R. E. Heiks, *J. Am. Chem. Soc.*, 1941, ***63***, 562.
35 J. Ning, K. Men, G. Xiao, L. Wang, Q. Dai, B. Zou, B. Liu and G. Zou, *Nanoscale*, 2010, ***2***, 1699.
36 G. A. Tritsaris, B. D. Malone and E. Kaxiras, *J. Appl. Phys.*, 2013, ***113***, 233507-1.
37 D. D. Vaughn II, R. J. Patel, M. A. Hickner and R. E. Schaak, *J. Am. Chem. Soc.*, 2010, ***132***, 15170.
38 D. D. Vaughn II, S.-I. In, R. E. Schaak, *Acs Nano*, 2011, ***5***, 8852.
39 R. L. Rich, *Inorganic Reactions in Water*., Springer, Berlin, 2007.
40 C. G. Davies and J. D. Donaldson, *J. Chem. Soc. A.*, 1968, 946.
41 A. Kergommeaux, M. Lopez-Haro, S. Pouget, J. –M, Zuo, C. Lebrun, F. Chandezon, D. Aldakov and P. Reiss, *J. Am. Chem. Soc.*, 2015, **137**, 9943.
42 A. J. Biacchi, D. D. Vaughn II and R. E. Schaak, *J. Am. Chem. Soc.*, 2013, ***135***, 11634.
43 L. A. Burton and A. Walsh, *J. Phys. Chem. C*, 2012, ***116***, 24262.